MANAS Journal of Engineering
ISSN 1694-7398 | e-ISSN 1694-7398

*Volume 8 (Issue 1) (2020) Pages 1-10*

# Carbon nanotube supported direct borohydride fuel cell anode catalysts: the effect of catalyst loading

Hilal Demir Kıvrak[1,*], Aykut Caglar[1], Tulin Avcı Hansu[1,2], Omer Sahin[2]

[1]Department of Chemical Engineering, Faculty of Engineering, Van Yuzuncu Yil University, Van, Turkey, hilalkivrak@gmail.com, hilalkivrak@yyu.edu.tr, ORCID: 0000-0001-8001-7854, ORCID: 0000-0002-0681-1096

[2]Department of Chemical Engineering, Faculty of Engineering, Siirt University, Siirt, Turkey, ORCID: 0000-0001-5441-4696, ORCID: 0000-0003-4575-3762

**ABSTRACT**

Energy, vital and permanent need for human life and welfare, supplied by fossil fuels such as oil, coal, and natural gas through the world has been rising gradually. However, the employment of fossil fuels to supply energy need have several disadvantages such as shortage of fossil fuels and global warming caused via fossil fuel exhaust gases. To eliminate these disadvantages of fossil fuel consumption in energy generating systems, research studies are dedicated to the alternative energy sources such as fuel cells, batteries, solar energy, wind energy. Fuel cells are the most popular alternative energy devices and attributed great importance to recompense the rapidly increasing energy demand. Direct Borohydride Fuel Cells (DBFCs), known as a special group of an alkaline direct liquid fuel cell (DLFC). At present, monometallic CNT supported Pd electrocatalysts (Pd/CNT) are prepared at varying Pd loadings via sodium borohydride (NaBH4) reduction method to investigate their NaBH4 electrooxidation activities. These monometallic Pd/CNT catalysts are characterized by X-ray Diffraction (XRD), N2 adsorption-desorption, X-ray photoelectron spectroscopy (XPS), and Scanning Electron Microscopy-Energy Dispersive X-ray analysis (SEM-EDX). NaBH4 electrooxidation measurements are performed with cyclic voltammetry (CV), chronoamperometry (CA), and electrochemical impedance spectroscopy (EIS). The 30% Pd/CNT catalyst exhibits the highest electrochemical activity. By altering Pd loading, catalyst surface electronic structure changes significantly, leading to enhanced NaBH4 electrooxidation activity. As a conclusion, it is clear that Pd/CNT catalysts are good candidate as anode catalysts for direct borohydride fuel cells.

**ARTICLE INFO**

***Research article***

*Received: 13.04.2020*
*Accepted: 27.05.2020*

***Keywords:***
*Pd/CNT,*
*fuel cell,*
*sodium borohydride,*
*catalyst,*
*loading*

**Corresponding author*

## 1. Introduction

Energy is one of the most important needs for the daily life and development and survival of human society. The emissions from fossil fuels cause toxic and dangerous substances, leading to serious environmental problems. Increasing global energy consumption has been caused exhausting of fossil fuels, leading to the search for alternative energy resources [1, 2]. The importance of renewable energy sources has enhanced global energy demand owing to the effects of petroleum-based fuels such as environmental pollution and global warming [3]. Fuel cells are the most popular alternative energy devices and attributed great importance to recompense the rapidly increasing energy demand [4]. Considering fuel cell, the chemical energy of molecules is converted into electrical energy with high energy efficiency [5, 6].

Polymer electrolyte membrane (PEM) fuel cells are commonly regarded as a competent substitute to batteries for portable power devices. Hydrogen PEM ($H_2$-PEM) fuel cells [7], direct methanol fuel cells (DMFCs) [8, 9], direct ethanol fuel cells (DEFCs), direct alcohol fuel cells (DAFCs) [10, 11], and direct formic acid fuel cells (DFAFCs) [12, 13] are most commonly studied fuel cells in literature. The critical limitations for commercialization of $H_2$-PEM are the high cost of miniaturized $H_2$ containers, potential dangers in the transportation of $H_2$, and low gas-phase energy density of $H_2$. Although liquid-alcohols have superior energy density compared to $H_2$, the toxicity of methanol vapor is still a remaining concern for the commercialization of DMFCs for on-board systems. On the other hand, C-C bond breaking is difficult for other alcohols [14, 15]. Due to some limitations in alcohol fuel cells such as $CO_2$ generation, low

electrochemical activity, and crossover, the researchers concentrated on Direct Borohydride Fuel Cells (DBFCs), known as a special group of an alkaline direct liquid fuel cell (DLFC) [16-18]. This kind of fuel cell produces electricity via the oxidation of borohydride anion ($BH_4^-$) at the anode and oxygen reduction at the cathode shown as Eq. (1.1) and Eq. (1.2) [19-21].

$$BH_4^- + 8OH^- \longrightarrow BO_2^- + 6H_2O + 8e^- \quad (E^0 = -1.24\ V) \quad (1.1)$$

$$O_2 + 2H_2O + 4e^- \longrightarrow 4OH^- \quad (E^0 = 0.40\ V) \quad (1.2)$$

Nanomaterials have attained much attention due to versatile applications such as disease diagnostics, photocatalysis, energy, environment, and storage appliances [22-27]. DBFCs have enhanced performances, especially regarding mobile applications [17, 28, 29]. In order to improve DBFC performance, the anode catalyst is one of the important elements to enhance its catalytic performance [30, 31]. The catalytic electrooxidation of $NaBH_4$ has been widely investigated by using various catalysts such as Pt [32-36], Au [37-40], Pd [41-43], Ag [44], Co [45-47], Ni [18], and alloys such as Pt–Bi [48], Pd–Bi [48], Pt-Ni [16, 49], Pt-Au [50], Pd-Au [51], Ni-Co [52], Cu-Ag [53]. There numerous studies on the synthesis, the characterization of CNT supported Pd catalysts and the investigation of their $NaBH_4$ electrooxidation activities. However, the mechanism of $NaBH_4$ electrooxidation has not still understood. Thus, the detailed investigation of CNT supported Pd catalysts should be performed to understand the mechanism.

Herein, monometallic CNT supported Pd electrocatalysts (Pd/CNT) are prepared at varying Pd loadings via the $NaBH_4$ reduction method to investigate their $NaBH_4$ electrooxidation activities. The electrochemical performance of Pd metal charges ranging from 0.1-70% by weight on the support material is investigated. The surface properties and electrochemical performances of these catalysts were examined with different techniques. Particle size and distribution of the Pd/CNT catalyst were defined by using XRD and SEM-EDX analysis. $N_2$ adsorption-desorption analysis was applied to check the surface area of the Pd/CNT catalyst. XPS spectroscopy was used to examine the possible chemical state of Pd in the Pd/CNT. The electrochemical activity of these catalysts was investigated by CV, CA, and EIS. Pd/CNT catalyst can be a promising anode catalyst for DBFCs with its high electrocatalytic performance and stability.

## 2. Experimental

### *2.1. Materials and equipments*

Potassium tetrachloropalladate (II) ($K_2PdCl_4$, 99.99%), sodium borohydride ($NaBH_4$, >99%), sodium hydroxide (NaOH, >98%), multi-walled carbon nanotube (MWCNT, 98%) were purchased from Sigma-Aldrich and used as received. Nafion 117 solution (5%) was obtained from Aldrich. Potentiostat, Ag/AgCl reference electrode, glassy carbon, and Pt wire electrodes were purchased from CH Instruments. Deionized water was distilled by the water purification system (Milli-Q Water Purification System). All glassware was washed with acetone and copiously rinsed with distilled water.

### *2.2. Preparation of catalysts and working electrodes*

#### *2.2.1. Preparation of monometallic catalysts*

The Pd/CNT catalyst was synthesized with the $NaBH_4$ reduction method. The metal loading on the carbon support was varied at 0.1-70 wt% Pd metal precursor ($K_2PdCl_4$) was dissolved in pure water and then CNT was added. These mixtures were stirred for two hours. $NaBH_4$ was used for metal reduction. After adding $NaBH_4$, stirring was continued for half an hour and filtered. Finally, these catalysts were washed completely and dried at 85 $^oC$ for 12 hours [54-56].

#### *2.2.2 Preparation of working electrodes*

Glassy carbon electrode was polished by alumina before electrode preparation. 5 mg of catalyst was dispersed in 1 mL of Aldrich 5% Nafion solution. As a result, a catalyst ink was obtained. Following this, 5 µL of the catalyst ink was dropped on a glassy carbon electrode. Finally, the electrode was dried at room temperature to remove the solvent.

### *2.3. Characterization techniques*

Monometallic 30% Pd/CNT catalyst was characterized by XRD, $N_2$ adsorption-desorption, SEM-EDX, and XPS measurements. XRD measurement of this catalyst was analyzed using a PANalytical Empyrean X-ray diffractometer device with Cu Kα radiation (λ = 1.54056 Å). $N_2$ adsorption-desorption analysis was conducted on a MicromeriticsTristar II 3020 equipped with surface area and porosity measurement analyzer that employed the BET method. XPS analysis was applied by the Specs-Flex device to determine the oxidation state of the Pd/CNT catalyst. SEM-EDX and mapping were analyzed employing the ZEISS SIGMA 300 to scan the surface of the Pd/CNT catalyst.

### *2.4. Electrochemical Measurements*

The electrochemical measurements of monometallic Pd/CNT catalysts were performed with CHI 660 E electrochemical potentiostat in a three-electrode system. The counter electrode was Pt wire and Ag/AgCl electrode was served as the reference electrode. The glassy carbon electrode was employed as the working electrode. All electrochemical measurements were performed in the cell at room temperature. The cyclic voltammograms were recorded in a

potential range of -1.0~0.4 V versus Ag/AgCl at a sweep rate of 50 mV $s^{-1}$ in 3 M NaOH + 0.1 M $NaBH_4$. Stability measurements of these catalysts were carried out in a 3 M NaOH + 0.1 M $NaBH_4$ solution with 600 s -0.4 V by CA. EIS as a dynamic method was used to examine the electrochemical behavior of catalysts. Then, Potentiostatic EIS measurements were recorded between 300 kHz and 0.04 Hz in 3 M NaOH + 0.1 M $NaBH_4$ at an amplitude of 5 mV at the -0.4 V electrode potential.

## 3. Results and discussion

### *3.1. Physical characterization*

XRD pattern of the Pd/CNT catalyst was illustrated in Figure 1. Figure 1 shows the diffraction peaks at 2Θ value of 25.7º, 39.5º, 45.6º, 67.0º, 80.7º, and 85.0º corresponding the C (0 0 2), Pd (1 1 1), Pd (2 0 0), Pd (2 2 0), Pd (3 1 1), and Pd (2 2 2) planes, respectively (JCPDS card no: 87-0638). These planes approve the existence of metallic Pd with face center cubic structure [57]. XRD line corresponding to (111) plane was observed to be intense according to other planes. Therefore, the crystallite size of this plane was calculated utilizing the Scherrer equation. The crystallite size corresponding to (111) plane was found as 5.87 nm.

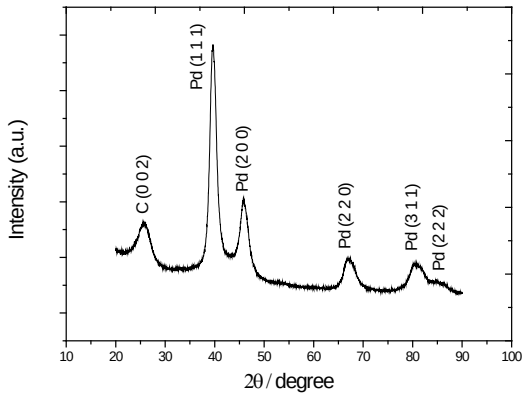


**Figure 1.** *XRD pattern of Pd/CNT catalyst.*

The $N_2$ adsorption-desorption analysis was used to characterize the BET surface area, average particle, and pore volume of the Pd/CNT catalyst and given in Figure 2. Union of Pure and Applied Chemistry (IUPAC) classifies hysteresis loops into H1, H2, H3, and H4 types [58]. Pd/CNT catalyst shows the V adsorption isotherms with an H1-type hysteresis loop which is usually connected to the pore duct with uniform size and regular shape [8, 59]. The average pore size, pore volume, and BET surface area of Pd/CNT were found as 24.5 nm, 0.93 $cm^3/g$, and 129.48 $m^2/g$, respectively.

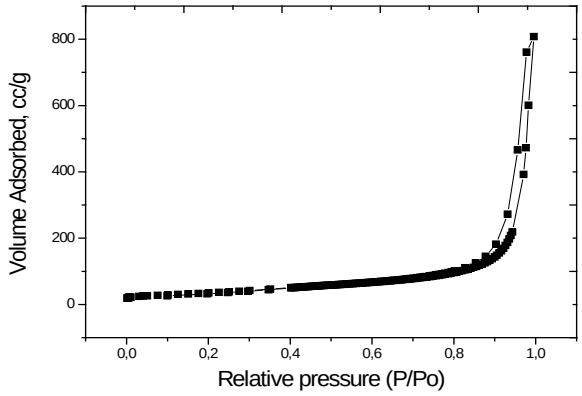


**Figure 2.** *$N_2$ adsorption-desorption isotherm of Pd/CNT catalyst.*

The possible chemical states of Pd in the Pd/CNT catalyst were defined via XPS and related spectra were illustrated in Figure 3. The deconvoluted Pd 3d spectra composed of six peaks at the presence of $Pd^0$ (Pd $3d_{5/2}$ at 335.7 eV and Pd $3d_{3/2}$ at 339.5 eV), PdO (Pd $3d_{3/2}$ at 341.0 eV), $Pd(OH)_x$ (Pd $3d_{5/2}$ at 336.3 eV and Pd $3d_{3/2}$ at 340.3 eV), and $PdO_2$ (Pd $3d_{5/2}$ at 337.4 eV). The elemental state ($Pd^0$) had a chemical state with a relative intensity of about 35% as well as the hydroxyl group.

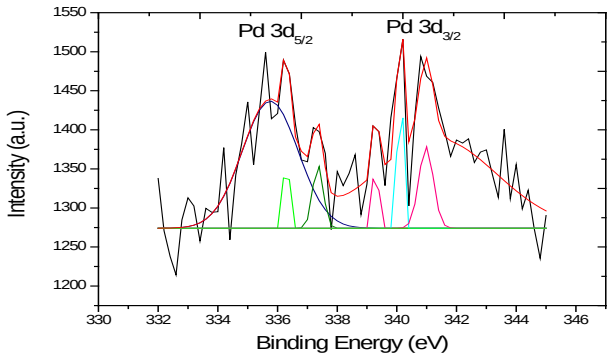


**Figure 3.** *XPS spectra of Pd/CNT.*

SEM-EDX and mapping images of the Pd/CNT catalyst was shown in Figure 4(a-e). This analysis was performed to set light to the formation and morphologies of the Pd/CNT catalyst. The Pd and carbon nanotube networks were plainly shown from Figure 4(a, b). In addition, it was observed that Pd metal was distributed homogeneously into the tube. The formation of the Pd/CNT catalyst was verified by mapping analysis in which turquoise and green particles indicate the Pd and carbon in Figure 4(c, d). The atomic and weight ratios from EDX results of Pd and carbon elements were given in Table 1. As shown in Table 1, the Pd metal was obtained on the carbon surface.

**Table 1**- *Atomic and weight elemental composition of the Pd/CNT catalyst.*

| Element | Weight % | Atomic % |
|---|---|---|
| C | 67.94 | 92.52 |
| O | 2.94 | 3.00 |
| Pd | 29.12 | 4.48 |

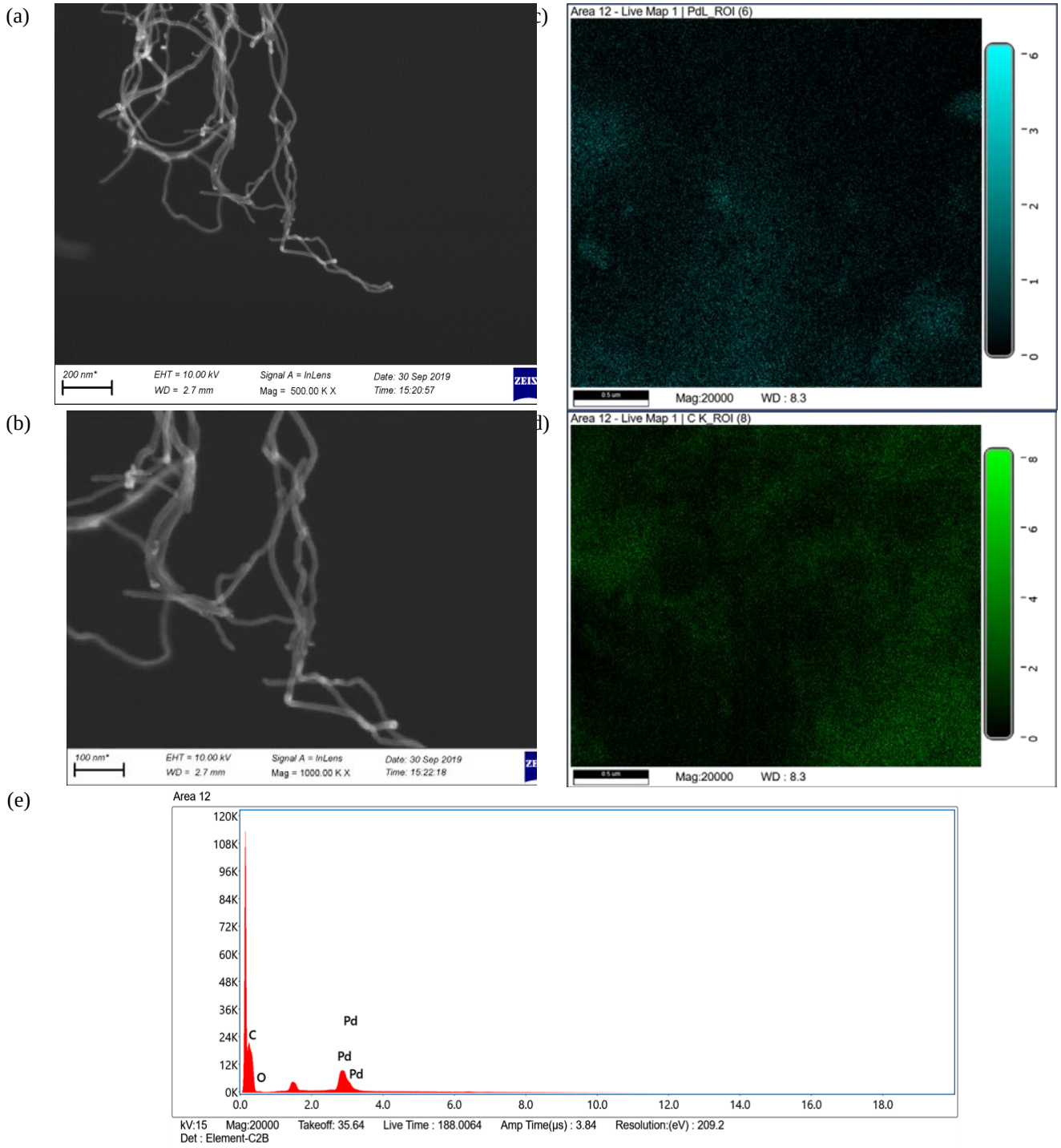


**Figure 4.** *SEM-EDX (a, b, e) and mapping images (Pd (c), C (d))of Pd/CNT catalyst.*

*3.2. Electrochemical measurements*

The electrochemical characterization of monometallic Pd/CNT electrocatalysts were evaluated by cyclic voltammetry at 3 M NaOH solution at 25 °C. Cyclic voltammograms were performed at -1.0 V ~ 0.4 V potential windows at 50 mV $s^{-1}$ scan rate for monometallic Pd/CNT electrocatalysts. A comparison of the cyclic voltammetric behaviors of monometallic Pd/CNT electrocatalysts were presented in Figure 5a. The highest current value of hydrogen adsorption-desorption peaks was obtained for the 70% Pd/CNT catalyst. The electrochemical active surface area (ECSA) of the synthesized 0.1-70.0% Pd/CNT catalysts were obtained from the $Q/(0.424*Pd_m)$ equation. Q (mC) is an area of the reduction of PdO peak, the 0.424 ($mC/cm^2$) charge is the reduction charge value associated with a monolayer of PdO, and $Pd_m$ is the Pd mass loading (mg). ECSA values of 0.1% Pd/CNT, 0.5% Pd/CNT, 1% Pd/CNT, 3% Pd/CNT, 5% Pd/CNT, 7% Pd/CNT, 10% Pd/CNT, 20% Pd/CNT, 30% Pd/CNT, 50% Pd/CNT, and 70% Pd/CNT catalysts were obtained as 551, 1336, 18, 115, 334, 216, 269, 280, 286, 309, and 260 $m^2/g$, respectively. On the other hand, activities of $NaBH_4$ electrooxidation reaction on monometallic Pd/CNT electrocatalysts were examined by CV measurements in 3 M NaOH + 0.1 M $NaBH_4$ at room temperature. As shown in Figure 5b, during the positive scan, $NaBH_4$ electrooxidation on monometallic Pd/CNT electrocatalysts began at about −0.8 V, while an oxidation peak appeared at -0.2 V. Cyclic voltammogram of monometallic Pd/CNT electrocatalysts revealed a peak located at around -0.3 V during the back scan, attributed to the electrocatalytic reaction of the interim product ($BH_3OH^-$) [31, 35]. 30% Pd/CNT catalyst exhibited better activity than the other monometallic Pd/CNT electrocatalysts. In addition, 30% Pd/CNT electrocatalyst displayed electrocatalytic activity with a maximum current density of 16.5 mA $cm^{-2}$. The purpose of adding wt% Pd metal precursor to the support material is to change the specific surface area and electronic properties of the surface. The 30% Pd/CNT catalyst has a high specific surface area and different surface electronic properties which provides more active sites for the reaction. This phenomenon is called as structure sensitivity. The exchange current density value of 16.5 mA $cm^{-2}$ (7.9 A $cm^{-2}$ $mg^{-1}_{Pd}$) appraised for $NaBH_4$ electrooxidation for 30% Pd/CNT catalyst was higher than those reported as 1.38 mA $cm^{-2}$ for $NaBH_4$ electrooxidation on Pd/rGO-$Fe_3O_4$ catalyst by Martins et al [19]. In addition, this catalyst was higher than the current density of the Pd-rGO-C@TiC electrode (1.35 A $cm^{-2}$ $mg^{-1}_{Pd}$) raported by Chen et al [43].

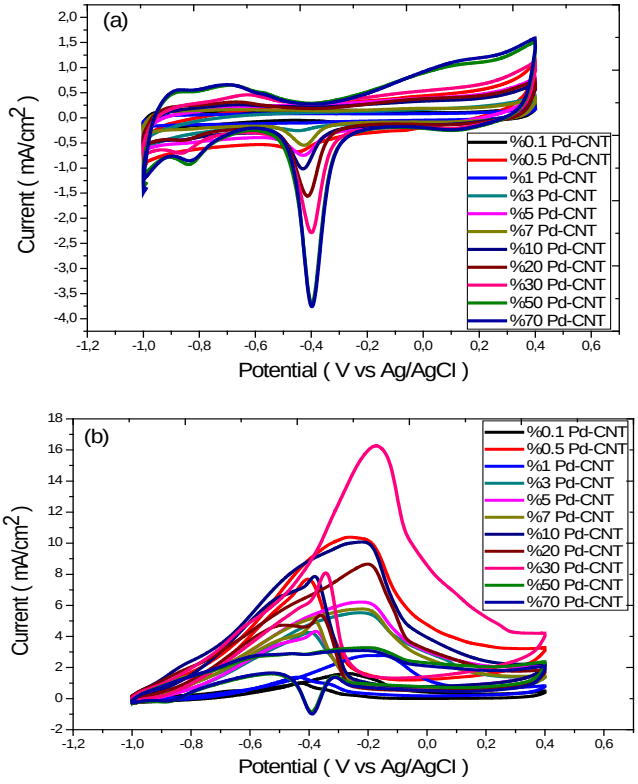


**Figure 5.** *Pd/CNT catalysts obtained (a) 3 M NaOH, (b) 3 M NaOH + 0.1 M $NaBH_4$ solution for cyclic voltammograms (scan rate: 50 mV $s^{-1}$).*

The stability and catalytic activity of 30% Pd/CNT catalysts at varying potentials were examined by using the CA method. Figure 6 shows the CA results of catalysts in the solution of 3 M NaOH + 0.1 M $NaBH_4$ at -0.4 V and -0.2 V potentials. The chronoamperometric curves display a sharp decrease in the first period owing to the accumulation of interim species at the surface of catalysts (Figure 6). As shown in Figure 6, the $NaBH_4$ electrooxidation of 30% Pd/CNT catalyst at -0.4 V indicates a higher initial current and a higher current at a longer time compared to other potentials. Furthermore, for the stability evaluation, the retention of the current value of 1000 s to the initial value was used by normalizing chronomaperommogram by dividing current values to initial current values and given in Figure 6b. Figure 6a and Figure 6b clearly shows that 30% Pd/CNT catalyst at -0.4 V potential has higher stability than the measurements at other potentials.

Nyquist plots obtained from EIS results were used to determine the $NaBH_4$ electrooxidation activity of 30% Pd/CNT catalyst. EIS measurements were performed between 300 kHz and 0.04 Hz in 3 M NaOH + 0.1 M $NaBH_4$ at an amplitude of 5 mV at the -0.4 V electrode potentials. According to the CV results, all catalysts have approximately -0.2 V peak currents. Therefore, CA analysis was taken at -0.2 and -0.4 V potentials. EIS measurements were taken at this potential as the best stability was achieved at -0.4 V. It is

understood that the image of the Nyquist plots is usually semicircle and the diameter of these semicircles is connected with the charge transfer resistance ($R_{ct}$) concerned with the electrocatalytic activity of electrocatalysts [60, 61]. As can be seen in Figure 7, since the 30% Pd/CNT catalyst has a smaller $R_{ct}$ than compared to the 5% Pd/CNT, 7% Pd/CNT, 10% Pd/CNT, and 50% Pd/CNT catalysts, it indicates that the $NaBH_4$ electrooxidation reaction increases in the 30% Pd/CNT catalyst [62].

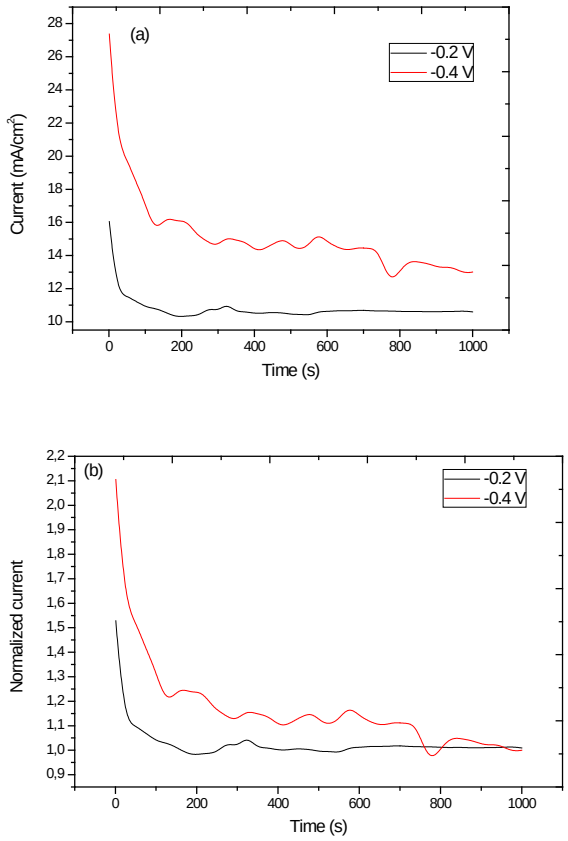


**Figure 6.** *(a) chronoamperomograms in solution of 3 M NaOH + 0.1 M $NaBH_4$ at -0.4 V and -0.2 V on 30% Pd/CNT catalyst (b) normalizing chronomaperommograms in solution of 3 M NaOH + 0.1 M $NaBH_4$ at -0.4 V and -0.2 V on 30% Pd/CNT catalyst.*

(a)

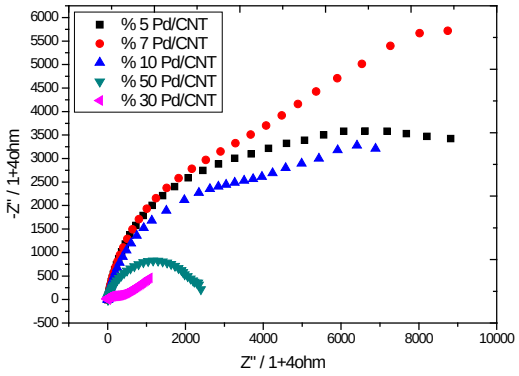


(b)

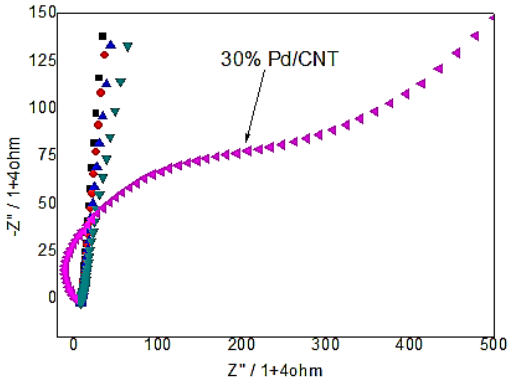


**Figure 7.** *Nyquist type EIS plots at -0.4 V potentials in 3 M NaOH + 0.1 M $NaBH_4$ on (a) Pd/CNT catalysts at various Pd loadings, (b) 30%Pd/CNT catalyst*

## 4. Conclusions

In this study, the monometallic Pd/CNT catalysts at varying 0.1-70.0% Pd loadings were prepared by the $NaBH_4$ reduction method. The 30% Pd/CNT catalyst was characterized via XRD, BET, SEM-EDX, and FTIR analyses. In addition, the monometallic Pd/CNT catalysts at varying 0.1 -70.0% were investigated by CV, CA, and EIS for $NaBH_4$ electrooxidation. The crystallite size corresponding to (111) plane is found as 5.87 nm for 30% Pd/CNT catalyst. The average pore size, pore volume, and BET surface area of Pd/CNT were found as 24.5 nm, 0.93 $cm^3/g$, and 129.48 $cm^2/g$, respectively. The 30% Pd/CNT catalyst has a high specific surface area and different surface electronic properties which provides more active sites for the reaction. This phenomenon is called as structure sensitivity [63]. An increase in Pd loading improves electrochemical activity until 30% Pd loading was reached. Further increase in Pd loading leads to a decrease in the electrocatalytic activity due to aggregation and blocking of the surface active sites. In this paper, the sample preparation method and its ultra-high electrocatalytic activity make Pd/CNT expected to be a promising electrode, which brings hope for the preparation of high-performance DBFCs [64].

**Acknowledgments**

The CHI 660E potentiostat employed in electrochemical measurements was purchased from the Scientific and Technological Research Council of Turkey (TUBITAK) project (project no: TUBITAK 113Z249). The chemicals were purchased from the Van YuzuncuYıl BAP project (project no: FBA-2018-7152). Characterization measurements were also purchased from Van Yuzuncu Yıl BAP project (project no: FBA-2018-7152).

**References**

[1]. Kurata M., Matsui N., Ikemoto Y., Tsuboi H., "Do determinants of adopting solar home systems differ between households and micro-enterprises? Evidence from rural Bangladesh", Renewable Energy, 129, (2018), 309-316.

[2]. Chia S.R., Ong H.C., Chew K.W., Show P.L., Phang S.-M., Ling T.C., Nagarajan D., Lee D.-J., Chang J.-S., "Sustainable approaches for algae utilisation in bioenergy production", Renewable Energy, 129, (2018), 838-852.

[3]. El-Nagar G.A., Derr I., Fetyan A., Roth C., "One-pot synthesis of a high performance chitosan-nickel oxyhydroxide nanocomposite for glucose fuel cell and electro-sensing applications", Applied Catalysis B: Environmental, 204, (2017), 185-199.

[4]. Hermann A., Chaudhuri T., Spagnol P., "Bipolar plates for PEM fuel cells: A review", International journal of hydrogen Energy, 30, (2005) 1297-1302.

[5]. Peighambardoust S.J., Rowshanzamir S., Amjadi M., "Review of the proton exchange membranes for fuel cell applications", International journal of hydrogen energy, 35 (2010) 9349-9384.

[6]. Hosseini H., Mahyari M., Bagheri A., Shaabani A., "Pd and PdCo alloy nanoparticles supported on polypropylenimine dendrimer-grafted graphene: a highly efficient anodic catalyst for direct formic acid fuel cells", Journal of Power Sources, 247, (2014) 70-77.

[7]. Brites Helú M.A., Fernandez W.V., Fernández J.L., "Ordered Array Electrodes Fabricated by a Mask-Assisted Electron-Beam Method as Platforms for Studying Kinetic and Mass-Transport Phenomena on Electrocatalysts", ChemElectroChem, 5, (2018) 2620-2629.

[8]. Ulas B., Caglar A., Kivrak A., Kivrak H., "Atomic molar ratio optimization of carbon nanotube supported PdAuCo catalysts for ethylene glycol and methanol electrooxidation in alkaline media", Chemical Papers, 73, (2019) 425-434.

[9]. Sahin O., Kivrak H., "A comparative study of electrochemical methods on Pt–Ru DMFC anode catalysts: The effect of Ru addition", International Journal of Hydrogen Energy, 38, (2013), 901-909.

[10]. Atbas D., Çağlar A., Kivrak H., Kivrak A., "Microwave Assisted Synthesis of Sn Promoted Pt Catalysts and Their Ethanol Electro-oxidation Activities", American Journal of Nanomaterials, 4, (2016), 8-11.

[11]. Sahin O., Duzenli D., Kivrak H., "An ethanol electrooxidation study on carbon-supported Pt-Ru nanoparticles for direct ethanol fuel cells", Energy Sources, Part A: Recovery, Utilization, and Environmental Effects, 38, (2016), 628-634.

[12]. Ulas B., Caglar A., Sahin O., Kivrak H., "Composition Dependent Activity of PdAgNi Alloy Catalysts for Formic Acid Electrooxidation", Journal of Colloid and Interface Science, 532, (2018), 47-57.

[13]. Caglar A., Sahan T., Cogenli M.S., Yurtcan A.B., Aktas N., Kivrak H., "A novel Central Composite Design based response surface methodology optimization study for the synthesis of Pd/CNT direct formic acid fuel cell anode catalyst", International Journal of Hydrogen Energy, 43, (2018), 11002-11011.

[14]. Chen C., Xu H., Shang H., Jin L., Song T., Wang C., Gao F., Zhang Y., Du Y., "Ultrafine PtCuRh nanowire catalysts with alleviated poisoning effect for efficient ethanol oxidation", Nanoscale, 11, (2019), 20090-20095.

[15]. Wang Y., Zheng M., Sun H., Zhang X., Luan C., Li Y., Zhao L., Zhao H., Dai X., Ye J.-Y., "Catalytic Ru containing Pt3Mn nanocrystals enclosed with high-indexed facets: Surface alloyed Ru makes Pt more active than Ru particles for ethylene glycol oxidation", Applied Catalysis B: Environmental, 253, (2019), 11-20.

[16]. Hosseini M.G., Rashidi N., Mahmoodi R., Omer M., "Preparation of Pt/G and PtNi/G nanocatalysts with high electrocatalytic activity for borohydride oxidation and investigation of different operation condition on the performance of direct borohydride-hydrogen peroxide fuel cell", Materials Chemistry and Physics, 208, (2018), 207-219.

[17]. Olu P.-Y., Barros C.R., Job N., Chatenet M., "Electrooxidation of NaBH4 in Alkaline Medium on Well-defined Pt Nanoparticles Deposited onto Flat Glassy Carbon Substrate: Evaluation of the Effects of Pt Nanoparticle Size, Inter-Particle Distance, and Loading", Electrocatalysis, 5, (2014), 288-300.

[18]. Zhang D., Wang G., Yuan Y., Li Y., Jiang S., Wang Y., Ye K., Cao D., Yan P., Cheng K., "Three-dimensional functionalized graphene networks modified Ni foam based gold electrode for sodium borohydride electrooxidation", International Journal of Hydrogen Energy, 41, (2016), 11593-11598.

[19]. Martins M., Metin Ö., Sevim M., Šljukić B., Sequeira C.A.C., Sener T., Santos D.M.F., "Monodisperse Pd nanoparticles assembled on reduced graphene oxide-Fe3O4 nanocomposites as electrocatalysts for borohydride fuel cells", International Journal of Hydrogen Energy, 43, (2018), 10686-10697.

[20]. Song C., Li B., Cheng K., Y K., Zhu K., Cao D., Wang G., "Synthesis and investigation of a high-activity catalyst: Au nanoparticles modified metalic Ti microrods for NaBH4 electrooxidation", International Journal of Hydrogen Energy, 43, (2018), 3688-3696.

[21]. Lafforgue C., Atkinson R.W., Swider-Lyons K., Chatenet M., "Evaluation of carbon-supported palladium electrocatalysts for the borohydride oxidation reaction in conditions relevant to fuel cell operation", Electrochimica Acta, 341, (2020), 135971.

[22]. Ajmal S., Bibi I., Majid F., Ata S., Kamran K., Jilani K., Nouren S., Kamal S., Ali A., Iqbal M., "Effect of Fe and Bi doping on LaCoO3 structural, magnetic, electric and catalytic properties", Journal of Materials Research and Technology, 8, (2019), 4831-4842.

[23]. Bibi I., Hussain S., Majid F., Kamal S., Ata S., Sultan M., Din M.I., Iqbal M., Nazir A., "Structural, dielectric and magnetic studies of perovskite [Gd1− xMxCrO3 (M= La, Co, Bi)] nanoparticles: photocatalytic degradation of dyes", Zeitschrift für Physikalische Chemie, 233, (2019), 1431-1445.

[24]. Majid F., Malik A., Ata S., Hussain Z., Bibi I., Iqbal M., Rafay M., Rizvi H., "Structural and Optical Properties of Multilayer Heterostructure of CdTe/CdSe Thin Films", Zeitschrift für Physikalische Chemie, 233, (2019), 1215-1231.

[25]. Majid F., Rauf J., Ata S., Bibi I., Yameen M., M. Iqbal, Hydrothermal Synthesis of Zinc Doped Nickel Ferrites: Evaluation of Structural, Magnetic and Dielectric Properties, Zeitschrift für Physikalische Chemie, 233, (2019), 1411-1430.

[26]. Majid F., Nazir A., Ata S., Bibi I., Mehmood H.S., Malik A., Ali A., Iqbal M.,"Effect of Hydrothermal Reaction Time on Electrical, Structural and Magnetic Properties of Cobalt Ferrite", Zeitschrift für Physikalische Chemie, (2019).

[27]. Aal R.M.A., Gitru M.A., Essam Z.M., "Novel synthetized near infrared cyanine dyes as sensitizer for dye sensitized solar cells based on nano-TiO2", Chemistry International, 3, (2017), 358-367.

[28]. Pramanik H., Rathoure A.K., "Electrooxidation study of NaBH4 in a membraneless microfluidic fuel cell with air breathing cathode for portable power application", International Journal of Hydrogen Energy, 42, (2017), 5340-5350.

[29]. Yang F., Cheng K., Ye K., Wei X., Xiao X., Guo F., Wang G., Cao D., "High performance of Au nanothorns supported on Ni foam substrate as the catalyst for NaBH4 electrooxidation", Electrochimica Acta, 115, (2014), 311-316.

[30]. Ye K., Ma X., Huang X., Zhang D., Cheng K., Wang G., Cao D., "The optimal design of Co catalyst morphology on a three-dimensional carbon sponge with low cost, inducing better sodium borohydride electrooxidation activity", RSC Advances, 6, (2016), 41608-41617.

[31]. D. Duan, Yin X., Wang Q., Liu S., Wang Y., "Performance evaluation of borohydride electrooxidation reaction with ternary alloy Au–Ni–Cu/C catalysts", Journal of Applied Electrochemistry, 48, (2018), 835-847.

[32]. Šljukić B., Milikić J., Santos D.M.F., Sequeira C.A.C., "Carbon-supported Pt0.75M0.25 (M=Ni or Co), electrocatalysts for borohydride oxidation", Electrochimica Acta, 107, (2013), 577-583.

[33]. Jin W., Liu J., Wang Y., Yao Y., Gu J., Zou Z., "Direct NaBH4–H2O2 fuel cell based on nanoporous gold leaves", International Journal of Hydrogen Energy, 38, (2013), 10992-10997.

[34]. Ojani R., Raoof J.-b., Valiollahi R., "Pt nanoparticles/graphene paste electrode for sodium borohydride electrooxidation", Journal of Solid State Electrochemistry, 17, (2013), 217-221.

[35]. Šljukić B., Milikić J., Santos D.M.F., Sequeira C.A.C., Macciò D., Saccone A., "Electrocatalytic performance of Pt–Dy alloys for direct borohydride fuel cells", Journal of Power Sources, 272, (2014), 335-343.

[36]. Oliveira R.C.P., Milikić J., Daş E., Yurtcan A.B., Santos D.M.F., Šljukić B., "Platinum/polypyrrole-carbon electrocatalysts for direct borohydride-peroxide fuel cells", Applied Catalysis B: Environmental, 238, (2018), 454-464.

[37]. Pe F.i, Wang Y., Wang X., He P.Y., Liu L., Xu Y., Wang H., "Preparation and Performance of Highly Efficient Au Nanoparticles Electrocatalyst for the Direct Borohydride Fuel Cell", Fuel Cells, 11, (2011), 595-602.

[38]. Santos D.M.F., Sequeira C.A.C., "Cyclic voltammetry investigation of borohydride oxidation at a gold electrode", Electrochimica Acta, 55, (2010), 6775-6781.

[39]. Olu P.-Y., Bonnefont A., Braesch G., Martin V., Savinova E. R., Chatenet M., "Influence of the concentration of borohydride towards hydrogen production and escape for borohydride oxidation reaction on Pt and Au electrodes – experimental and modelling insights", 2017.

[40]. Yan P., Zhang D., Cheng K., Wang Y., Ye K., Cao D., Wang B., Wang G., Li Q., "Preparation of Au nanoparticles modified TiO2/C core/shell nanowire array and its catalytic performance for NaBH4 oxidation", Journal of Electroanalytical Chemistry, 745, (2015), 56-60.

[41]. Cheng K., Xu Y., Miao R.R., Yang F., Yin J.L., Wang G.L., Cao D.X., "Pd Modified MmNi50.6Co10.2Mn5.4Al1.2 Alloy as the Catalyst of NaBH4 Electrooxidation", Fuel Cells, 12, (2012), 869-875.

[42]. Braesch G., Bonnefont A., Martin V., Savinova E.R., Chatenet M., "Borohydride oxidation reaction mechanisms and poisoning effects on Au, Pt and Pd bulk electrodes: From model (low) to direct borohydride fuel cell operating (high) concentrations", Electrochimica Acta, 273, (2018), 483-494.

[43]. Cheng K., Jiang J., Kong S., Gao Y., Ye K., Wang G., Zhang W., Cao D., "Pd nanoparticles support on rGO-C@TiC coaxial nanowires as a novel 3D electrode for NaBH4 electrooxidation", International Journal of Hydrogen Energy, 42, (2017), 2943-2951.

[44]. Sanli A.E., Aytaç A., Uysal B.Z., Aksu M.L., "Recovery of NaBH4 from BH3OH− hydrolyzed intermediate on the AgI surface treated with different electrochemical methods", Catalysis Today, 170, (2011), 120-125.

[45]. Zhang D., Ye K., Cao D., Wang B., Cheng K., Li Y., Wang G., Xu Y., "Co@MWNTs-Plastic: A novel electrode for NaBH4 oxidation", Electrochimica Acta, 156, (2015), 102-107.

[46]. Zhang D., Ye K., Cheng K., Cao D., Yin J., Xu Y., Wang G., "High electrocatalytic activity of cobalt–multiwalled carbon nanotubes–cosmetic cotton nanostructures for sodium borohydride electrooxidation", International Journal of Hydrogen Energy, 39, (2014), 9651-9657.

[47]. Guo S., Sun J., Zhang Z., Sheng A., Gao M., Wang Z., Zhao B., Ding W., "Study of the electrooxidation of borohydride on a directly formed CoB/Ni-foam electrode and its application in membraneless direct borohydride fuel cells", Journal of Materials Chemistry A, 5, (2017), 15879-15890.

[48]. Simões M., Baranton S., Coutanceau C., "Influence of bismuth on the structure and activity of Pt and Pd nanocatalysts for the direct electrooxidation of NaBH4", Electrochimica Acta, 56, (2010), 580-591.

[49]. Wang B., Zhang D., Ye K., Cheng K., Cao D., Wang G., Cheng X., "Plastic supported platinum modified nickel electrode and its high electrocatalytic activity for sodium borohydride electrooxidation", Journal of Energy Chemistry, 24, (2015), 497-502.

[50]. Iotov P.I., Kalcheva S.V., Kanazirski I.A., "On the enhanced electrocatalytic performance of PtAu alloys in borohydride oxidation", Electrochimica Acta, 108, (2013), 540-546.

[51]. Simões M., Baranton S., Coutanceau C., "Electrooxidation of Sodium Borohydride at Pd, Au, and PdxAu1−x Carbon-Supported Nanocatalysts", The Journal of Physical Chemistry C, 113, (2009), 13369-13376.

[52]. Guo M., Cheng Y., Yu Y., Hu J., "Ni-Co nanoparticles immobilized on a 3D Ni foam template as a highly efficient catalyst for borohydride electrooxidation in alkaline medium", Applied Surface Science, 416, (2017), 439-445.

[53]. Duan D., Liu H., Wang Q., Wang Y., Liu S., "Kinetics of sodium borohydride direct oxidation on carbon supported Cu-Ag bimetallic nanocatalysts", Electrochimica Acta, 198, (2016), 212-219.

[54]. Caglar A., Ulas B., Cogenli M.S., Yurtcan A.B., Kivrak H., "Synthesis and characterization of Co, Zn, Mn, V modified Pd formic acid fuel cell anode catalysts", Journal of Electroanalytical Chemistry, 850, (2019), 113402.

[55]. Caglar A., Kivrak H., "Highly active carbon nanotube supported PdAu alloy catalysts for ethanol electrooxidation in alkaline environment", International Journal of Hydrogen Energy, 44, (2019), 11734-11743.

[56]. Çağlar A., Aldemir A., Kivrak H., "Alcohol electrooxidation study on carbon nanotube supported monometallic, Pt, Bi, and Ru catalysts", Fullerenes, Nanotubes and Carbon Nanostructures, 26, (2018), 863-870.

[57]. Navaladian S., Viswanathan B., Varadarajan T.K., Viswanath R.P., "A Rapid Synthesis of Oriented Palladium Nanoparticles by UV Irradiation", Nanoscale Res Lett, 4, (2008), 181-186.

[58]. I.L.M. SIT, Characterızation of the structure and performance of Ce3+ exchanged lix molecular sieves, Materiali in tehnologije, 52, (2018), 423-428.

[59]. Ulas B., Caglar A., Kivrak H., "Determination of optimum Pd: Ni ratio for Pd x Ni 100-x/CNT s formic acid electrooxidation catalysts synthesized via sodium borohydride reduction method", International Journal of Energy Research, 43, (2019), 3436-3445.

[60]. Karuppasamy L., Chen C.-Y., Anandan S., Wu J.J., "Sonochemical fabrication of reduced graphene oxide supported Au nano dendrites for ethanol electrooxidation in alkaline medium", Catalysis Today, 307, (2018), 308-317.

[61]. Chen S., Xu H., Yan B., Li S., Dai J., Wang C., Shiraishi Y., Du Y., "Highly active electrooxidation of ethylene glycol enabled by pinecone-like Pd–Au–Ag nanocatalysts", Journal of the Taiwan Institute of Chemical Engineers, 83, (2018), 64-73.

[62]. Xu H., Song P., Yan B., Wang J., Gao F., Zhang Y., Du Y., "Superior ethylene glycol electrocatalysis enabled by Au-decorated PdRu nanopopcorns", Journal of Electroanalytical Chemistry, 814, (2018), 31-37.

[63]. Zhang J., Zhang D., Cui C., Wang H., Jiao W., Gao J., Liu Y., "A three-dimensional porous Co–P alloy supported on a copper foam as a new catalyst for sodium borohydride electrooxidation", Dalton Transactions, 48, (2019), 13248-13259.

[64]. Yin X., Wang Q., Duan D., Liu S., Wang Y., "Amorphous NiB alloy decorated by Cu as the anode catalyst for a direct borohydride fuel cell", International Journal of Hydrogen Energy, 44, (2019), 10971-10981.